UNIVERSITY COLLEGE LONDON

Department of Electronic and Electrical Engineering

Advanced Semiconductor Lasers Using the Quantum Confined Stark Effect Tuning Mechanism

Contract F61708-97-W0204

Final Report

prepared by

Oliver Gough, Oliver Berger, Ju-Bin Song and Alwyn Seeds

July, 1999

TORRINGTON PLACE LONDON WC1E 7JE UK
Telephone: +44 171-380 7928
Facsimile: +44 171-387 4350
e-mail: a.seeds @ ee.ucl.ac.uk

Abstract

This is the final report for the first year of a programme to realise InP/InGaAsP tuneable lasers which use the quantum-confined Stark effect (QCSE) as a tuning mechanism to produce a fast and uniform tuning response.

To examine the potential for microwave rate tuning special two section low parasitic monolithically integrated GaAs/AlGaAs QCSE tuned lasers were fabricated, packaged on low parasitic sub-mounts and evaluated. Peak deviation > 10 GHz, FM amplitude response uniform within ± 2.5 dB from 30 kHz to 6 GHz, FM phase response uniform to within ± 20° over the same frequency range, intensity modulation less than 5%, linewidth less than 10 MHz and room temperature CW output power greater than 10 mW/facet were all successfully achieved. These results represent the widest and most uniform FM frequency response ever reported for a field effect tuned semiconductor laser. The upper frequency limit could be further extended with more complex fabrication techniques. Details of this work were given in the interim report for this contract.

A comprehensive model for multi-section lasers was developed using the TLLM approach. The modelling capability includes a number of different laser elements such as bulk active, quantum well active, passive, field effect tuned and Distributed Bragg Reflector (DBR) sections. The various sections can be cascaded and independently biased or modulated in order to model many different types of device. The model successfully predicts the characteristics of both the QCSE tuned lasers described above and InP/InGaAsP fibre grating lasers (FGLs).

We have focused our practical work on InP/InGaAsP lasers on characterising the QCSE induced refractive index changes in InP, the development of reliable processing technology and the characterisation of mesa-stripe lasers fabricated from MQW wafers grown both by MOVPE and by MBE to obtain detailed qualification data on the wafers used. Working with the growers at the University of Sheffield we have achieved lasers with competitive threshold current densities of around 400 A/cm^2 from unstrained material. With strained layer epitaxial material from the Laboratory for Physical Sciences we have obtained state of the art threshold current densities of below 250 A/cm^2. We have also successfully fabricated ridge-guide lasers from the MOVPE material with threshold currents below 70 mA.

Introduction

This project has as its objective the fabrication of advanced tunable laser structures in the InP/InGaAsP material system. The tuning mechanism to be explored is the Quantum Confined Stark Effect (QCSE) through the reverse biassing of multiple quantum well intra-cavity elements. The work in this project is substantially based on the development of monolithically integrated, QCSE tuned, GaAs/AlGaAs based lasers which was carried out under previous AFOSR contracts.

The lasers previously reported had room temperature CW threshold currents below 20mA, CW output powers exceeding 10mW, and side mode suppression exceeding 20dB. The FM response uniformity was better than ±2.5dB over the range 10kHz to 2 GHz.

In the interim report for this contract we detailed the improvements in performance of these lasers which have been achieved through the development of air-bridge contacting techniques and by the use of Aluminium Nitride microstrip submounts for the lasers. The resulting reduction in parasitic capacitances has allowed the extension of the upper frequency limit. The FM response magnitude uniformity in these laser has been found to be better than ±3dB over the range 30 kHz to 6 GHz. The FM response phase was also uniform to within ± 20° over the same frequency range, with the frequency change in phase with the modulating signal voltage. These results represent the widest and most uniform FM frequency response ever reported for a field effect tuned semiconductor laser. We also characterised the linewidth performance of these lasers, achieving a linewidth of about 10 MHz, nearly independent of tuning section bias. These measurements conclude our work on GaAs/AlGaAs tunable lasers in which we have exceeded all of the stated contract objectives.

Turning to the work on InGaAsP lasers, we have developed a simulation which allows the modelling of multi-section semiconductor lasers. The program models the devices in the time domain, with spectral information obtained via fast Fourier transform (FFT). The modelling capability includes a number of different laser elements such as bulk active, quantum well active, passive, field effect tuned and Distributed Bragg Reflector (DBR) sections. The various sections can be cascaded and independently biased or modulated in order to model many different types of device. This tool has been used to model proposed InGaAsP laser structures and shows good agreement with the measured results.

In our experimental programme, we have fabricated normal incidence InGaAs/InGaAsP test structures, which we have used to study the electric field dependent change in refractive index of this materials system, and hence estimate the potential tuning range of InGaAsP QCSE tuned

lasers. Measurement of the absorption spectra allow the determination of refractive index changes. These results can then be used to generate design parameters for multi-section tunable lasers as well as external cavity lasers. These results show that realistic monolithic devices can be produced with tuning section lengths of below 400 μm. This is an important point since to achieve high modulation bandwidths will require small capacitance i.e. short tuning sections.

We have also carried out extensive work to develop the fabrication technologies required for QCSE tuned ridge guide InGaAsP lasers. This work has been supported by characterisation of mesa-stripe lasers fabricated from MQW wafers grown both by MOVPE and by MBE to obtain detailed qualification data on the wafers used. Working with the growers at the University of Sheffield we have achieved lasers with competitive threshold current densities of around 400 A/cm^2 from unstrained material. With strained layer epitaxial material from the Laboratory for Physical Sciences we have obtained state of the art threshold current densities of below 250 A/cm^2. We have also successfully fabricated and characterised ridge guide InGaAsP lasers using University of Sheffield material, with threshold currents below 70mA. Crystallographic wet etch methods have been developed to fabricate ridges with good control over the ridge dimensions and profile. Other processing techniques implemented were gold electroplating and bromine/methanol based wafer thinning.

The report is organised into 4 chapters. The first chapter describes our work on the development of InGaAsP/InP ridge waveguide laser diodes. Chapter 2 describes our work on characterising the QCSE response of InGaAsP/InP MQW wafers. In Chapter 3 the Transmission Line Laser Model is introduced as a suitable tool for the dynamic modelling of multi-section laser devices and modelling results for structures of interest are presented. Finally Chapter 4 provides a summary of the work planned for the future in the area of advanced laser sources.

Chapter 1 Progress in InP based lasers.

1.1 Epitaxy

1.1.1 Wafer MR1080

This structure consists of 5 InGaAs quantum wells with quaternary barriers (λ=1.28μm) lattice matched to InP and was grown by MOVPE at the EPSRC III-V Central Facility, University of Sheffield. The p-type dopant is Zn with a nominal concentration of $6.0x10^{18}$ cm^{-3} in the contact layer and the n-type dopant is Si. A thin (150 nm) InGaAsP etch stop layer was grown 0.1um from the bottom of the p-type InP cladding layer to permit fabrication of the ridge using a selective etch technique. The nominal dopant concentrations and dimensions of the structure are shown in Figure 1.1(a). The actual carrier concentration in the cap layer was found to be $2.0x10^{18}$ cm^{-3}.

1.1.2 Wafer MR1205

This wafer has a similar epitaxial structure to MR1080. However, the doping concentrations have been changed. The doping concentration of the cap layer is reduced to $4.0x10^{18}$ cm^{-3} but since the measured carrier concentration in that layer was also $4.0x10^{18}$ cm^{-3}, an increase over MR1080, we expect an improvement in the contact resistance, at the same time the doping of the cladding layers is increased to reduce the overall series resistance of the diode. Again, a quaternary InGaAsP etch stop layer is inserted in the p-type cladding layer to make narrow ridge using selective etch. The nominal doping and layer thickness for this wafer is shown in Figure 1.1(b).

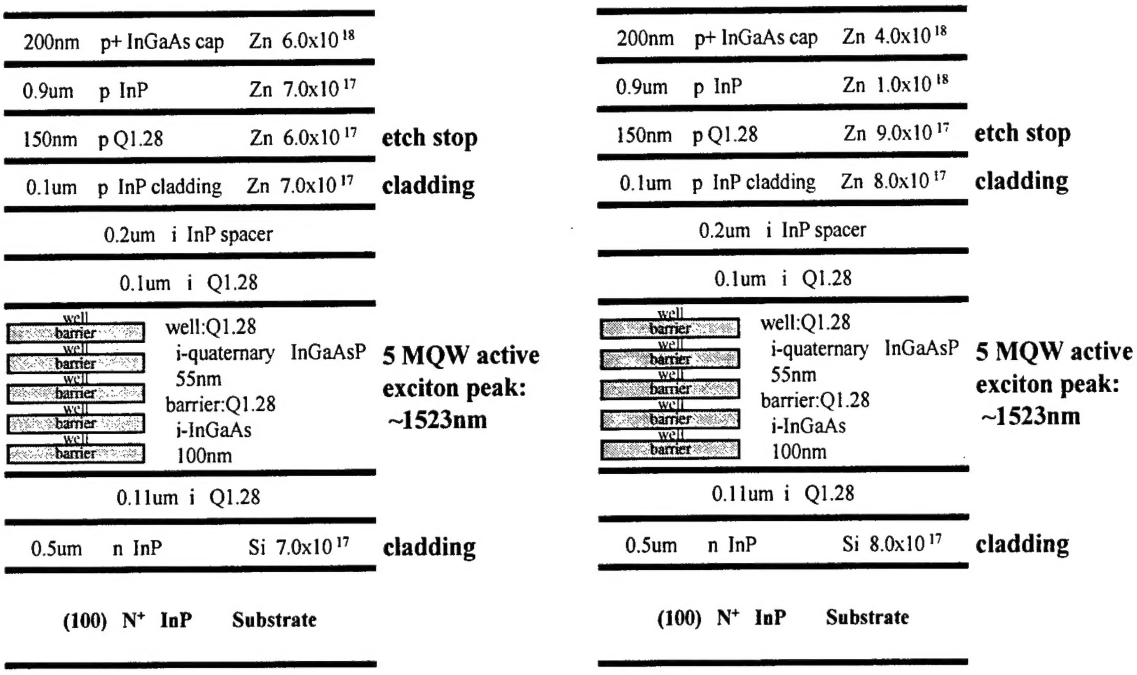

(a) Wafer MR1080 (b) Wafer MR1205

Figure 1.1: The epitaxial structures of wafers MR1080 and MR1205.

1.2 Processing of ridge waveguide structures

The development of reliable processing techniques is vital to the successful realisation of ridge waveguide lasers in the InGaAsP/InP material system. A number of issues were addressed in the process development. Of particular importance were the ridge definition problem and the contact metallisations.

1.2.1 Ridge definition

The ridge waveguide structure provides both optical and electrical confinement in the direction parallel to the junction. The depth of the ridge etch is important in controlling the shape of the optical mode. In the epitaxial structures used in this project a thin quaternary etch stop layer is included at the target etch depth. Using a selective etch will enable accurate formation of the ridge structure.

The ridge is formed on the epitaxial structure by a wet etching method. We investigated a number of etchants which result in anisotropic etch profiles due to their interaction with the crystal structure. The InGaAs cap layer was removed using an etch solution composed of $H_3PO_4/H_2O_2/H_2O$ in the ratio 8:1:1; this etch does not attack the InP cladding layers. The InP cladding layers are etched using a solution of HCl/H_3PO_4 (1:1). This solution distinguishes between the <110> and $<1\bar{1}0>$ directions on <100> InP producing a different etch profile when the ridge mask is aligned perpendicular or parallel to the major flat of the wafer.

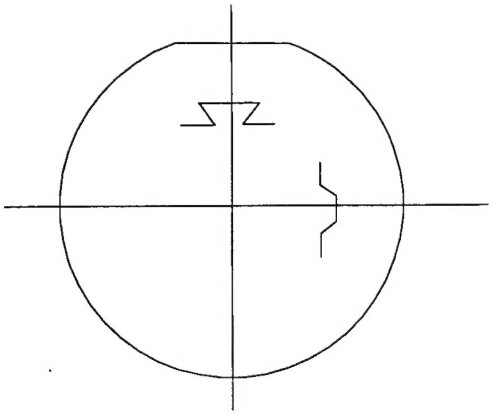

Figure 1.2: A schematic illustration of how the orientation of the ridge impacts the shape of the ridge.

The ridge shape obtained when the mask is aligned perpendicular to the major flat is a dovetail with a degree of underetch while in the orthogonal direction, parallel to the major flat, the shape is trapezoidal (see Figure 1.2). The trapezoidal etch profile is chosen as the most suitable for the ridge waveguide device. The trapezoidal ridge profile obatained is shown in Figure 1.3. The ridge width used for these devices was 4μm.

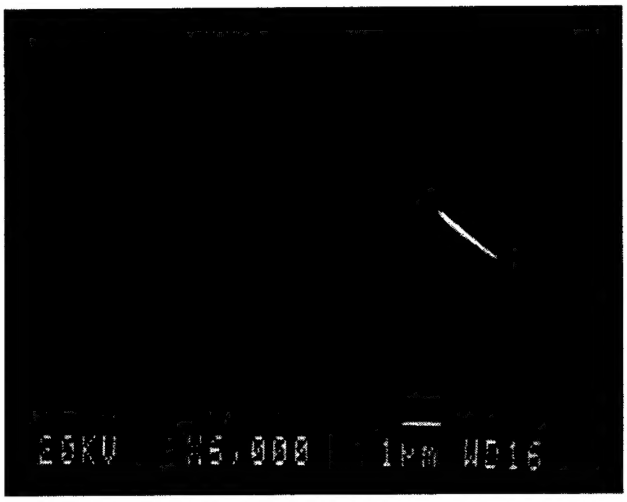

Figure 1.3: SEM photograph of the wet etched ridge profile aligned parallel to the major flat of the wafer.

1.2.2 Metallisation

The structure is passivated by depositing a 300 nm thick layer of silicon dioxide on the etched wafer using a PECVD (Plasma Enhanced Chemical Vapour Deposition) reactor. A contact window is etched on top of the ridge and the p-contact metallisation is deposited. We have used a two step metallisation process. The contact to the InGaAs cap layer is made using a thermally evaporated Au/Zn/Au metallisation which we have found to have a low contact resistivity, however this metal has poor adhesion to the passivation layer which can result in the metal delaminating at a later stage of the process. To prevent this, the Au/Zn/Au metal is patterned by a lift off technique so that it only remains on the contact holes on top of the ridge. A subsequent deposition of Ti/Au by thermal evaporation forms the large area bond pad .

1.2.3 Electroplating

The ridge etch results in the wafer surface being non-planar, and consequently the evaporated metal may be thin at the steps in the surface. This could lead to failure of the metal layer under high current drive. To combat this an unsmoothed DC electroplating process was developed to build up a thick gold layer on the bond pad. A thin layer of gold (30-50 nm) was evaporated on the surface to ensure all the areas to be plated were in good electrical contact. A photolithography stage followed

to mask the areas where electroplating is not desired. The wafer piece is mounted in the electroplating circuit (see Figure 1.4) and placed in the plating solution. Typical plating currents were 1.3 mA to plate a 1 cm^2 piece at a rate of 0.15 μm/min. A gold etch solution can be used to remove the thin gold layer that provided electrical connectivity.

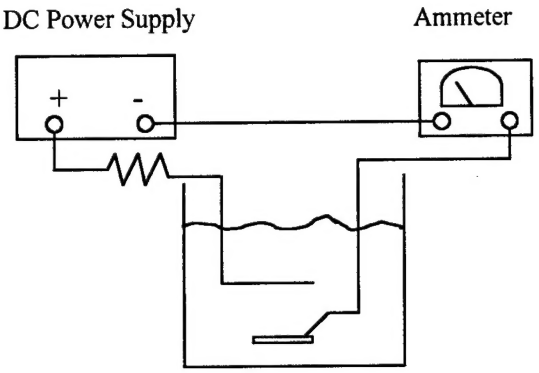

Figure 1.4: Schematic of the arrangement for DC plating of gold.

1.2.4 Wafer thinning

The wafer is subsequently thinned to a total thickness of approximately 100μm by a Bromine/Methanol bubble etch, which results in less mechanical damage to the wafer than mechanical polishing. The etch solution was 5 vol% bromine in methanol. Nitrogen was allowed to flow into the etch solution through a diffuser to produce a steady flow of bubbles (approx. 10sccm). The nitrogen prevents stagnation of the etch solution which can result in non uniform etch characteristics. The sample to be etched is attached to a glass slide using dental wax ensuring that the p side metallisation is completely protected. Care should be taken that the grade of wax is fully resistant to the etch solution (typically a wax with a melting point of >130°C will suffice). The sample is suspended in the etch solution for the required length of time, ideally in a horizontal position and being slowly rotated to ensure uniformity (Figure 1.5), as nitrogen bubbles tracking across the sample can result in trenching. For InP material the etch rate of freshly prepared solution is about 27 μm/min, however if the solution is used for a number of samples in succession the etch rate will decline to about 18 μm/min. Hence, in practice it is necessary to measure the etch rate for each sample. The etched samples are rinsed carefully in methanol. Finally the back contact

metallisation of AuGe/Au is evaporated. The wafer can then be cleaved into individual lasers for testing.

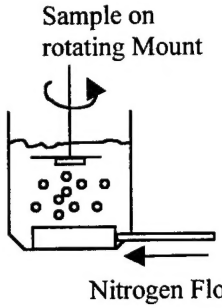

Figure 1.5: The arrangement for wafer thinning using a Bromine/Methanol bubble etch.

1.3 Electrical Characteristics

The electrical and optical characteristics of the cleaved ridge waveguide lasers were examined. The I-V characteristics were measured using a HP4145 parameter analyser.

For the p-type Zn doped InGaAs cap layer, Au/Zn/Au metal systems showed low contact resistance using the thermal evaporation technique. The specific contact resistance of the lasers was found to be $5x10^{-2}$ Ωcm^2 for MR1080 and in the case of MR1025 $3x10^{-4}$ Ωcm^2 was achieved.

Under forward bias, the slope of the I-V characteristic in the high current injection region is a good estimate of the contact and series resistance of the device (approximately 10Ω for the device shown in Figure 1.6) . The results of representative I-V traces from devices fabricated on wafers MR1080 and MR1025 are shown in Figures 1.6 to 1.8.

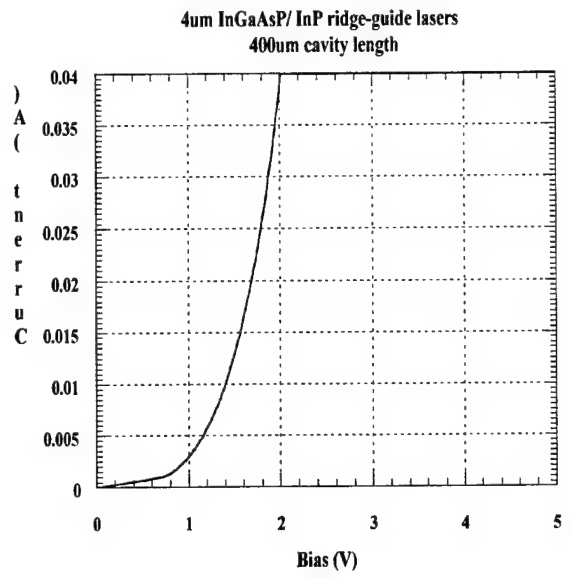

Figure 1.6: I-V characteristic of a ridge waveguide laser fabricated from MR1080.

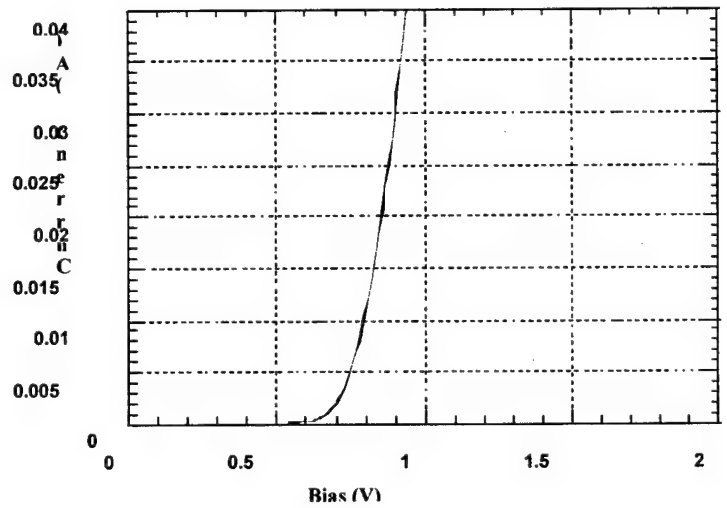

Figure 1.7: I-V characteristic of a 100 μm wide stripe laser fabricated from MR1080

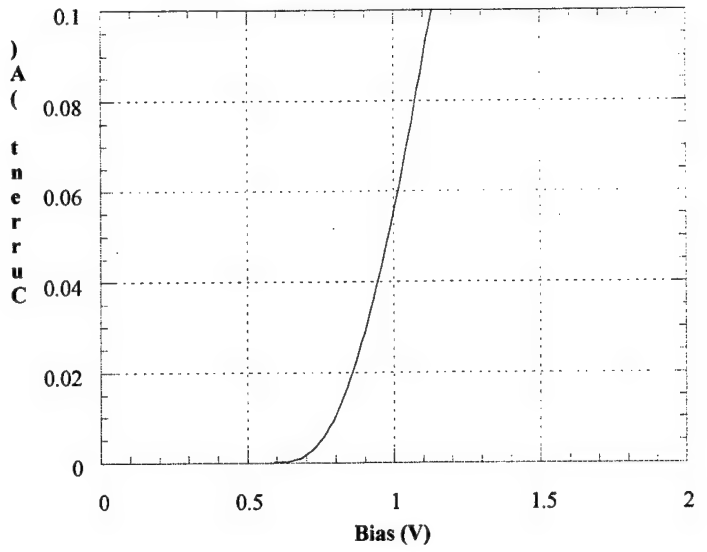

Figure 1.8: I-V characteristic of a 100 μm wide stripe laser fabricated from MR1205

1.4 Optical Characteristics

Initial L-I testing is carried out under pulsed conditions at a probe station to identify suitable devices for further analysis. The laser diodes are subsequently bonded to gold plated brass heat sinks for complete testing.

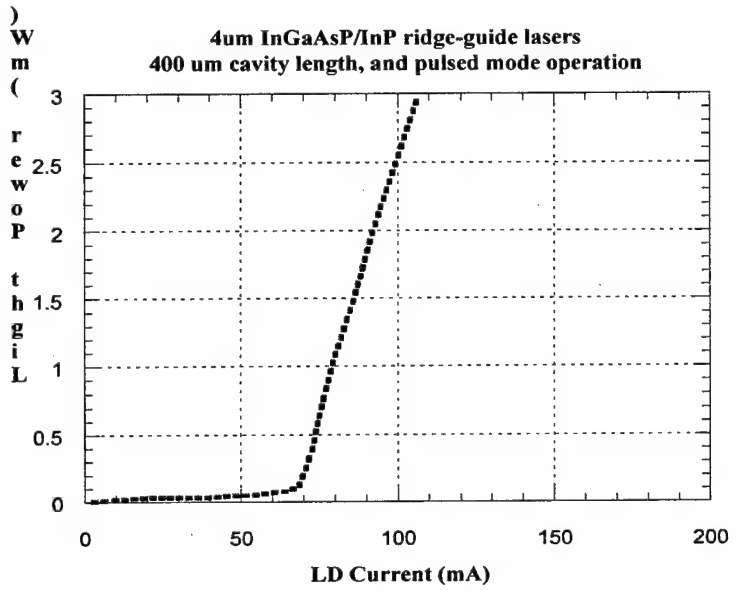

Figure 1.9:A representative L-I characteristics of R1080 ridge-guide lasers (Pulse length = 0.6 μs, Duty cycle = 1.2%)

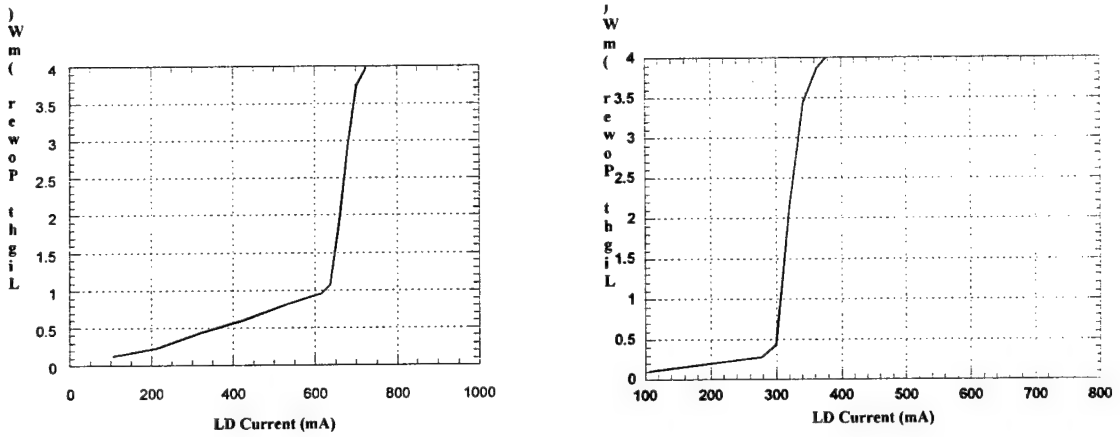

(a) (b)

Figure 1.10: L-I characteristics for stripe lasers from MR1080. (a) A 300 μm long 100 μm wide stripe device. (b) A 500 μm long 20 μm wide stripe device (Pulse length = 0.6 μs, Duty cycle = 1.2%)

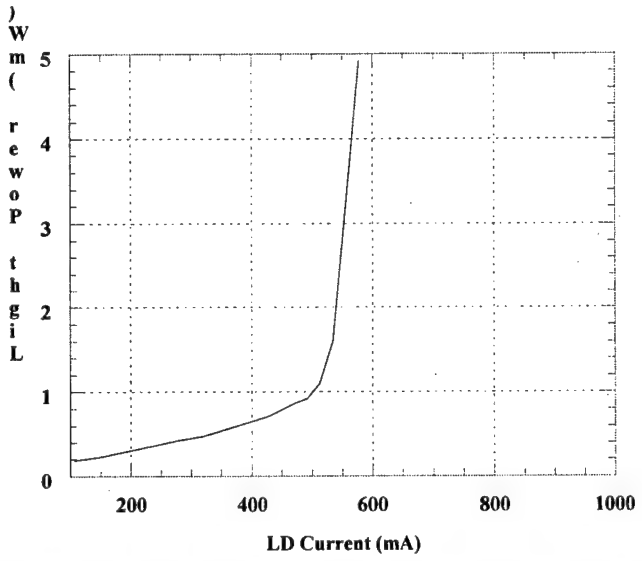

Figure 1.11: The L-I characteristic of a 100 μm stripe laser with a cavity length of 400 μm from wafer MR1205, (Pulse length = 0.6 μs, Duty cycle = 1.2%).

The optical power-injected current (L-I) characteristics which enables the determination of threshold current and its variation with temperature and cavity length has been studied. The measurement is carried out under pulsed operation and at room temperature. Figure 1.9 shows a typical L-I characteristic for a ridge waveguide laser fabricated from MR1080. The threshold current I(th) is

70mA for this 400μm cavity length laser. Figures 1.10 and 1.11 show the L-I characteristics of mesa stripe lasers fabricated from both MR1080 and MR1205. MR1205 seems to have an improved threshold current density in comparison to MR1080 (~ 1300 Acm^{-2} compared with ~1700 Acm^{-2}).

The threshold carrier density for an infinitely long cavity, J_∞ can be extrapolated from the threshold current density data of a group of lasers of different lengths. This can be used as an estimate of the transparency carrier density of the material. The J_∞ estimate in Figure 1.10 was made using 100 μm wide mesa stripe lasers from MR1080.

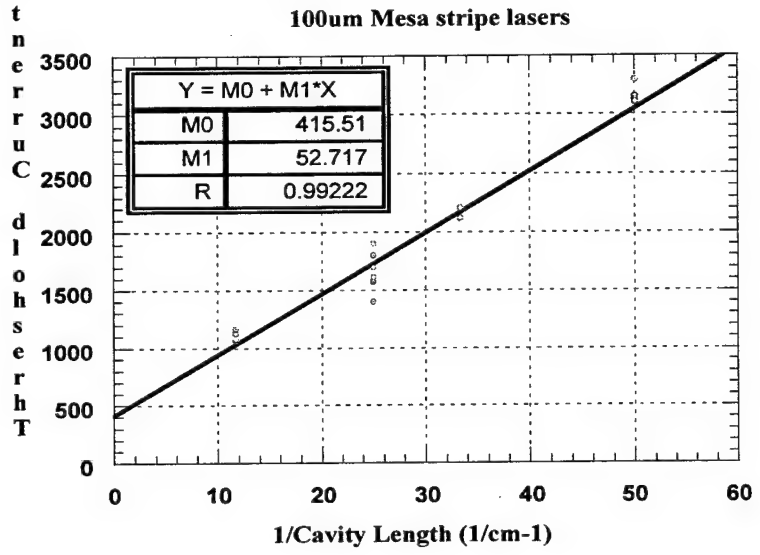

Figure 1.12: Threshold current density of MR1080 lasers (100μm stripe laser)

The spectrum of the MR1080 ridge guide laser is shown in Figure 1.13. The centre wavelength is at 1525 nm. This corresponds well with the peak emission wavelength of 1523 nm measured in a room temperature Photoluminescescence experiment (Figure 1.14).

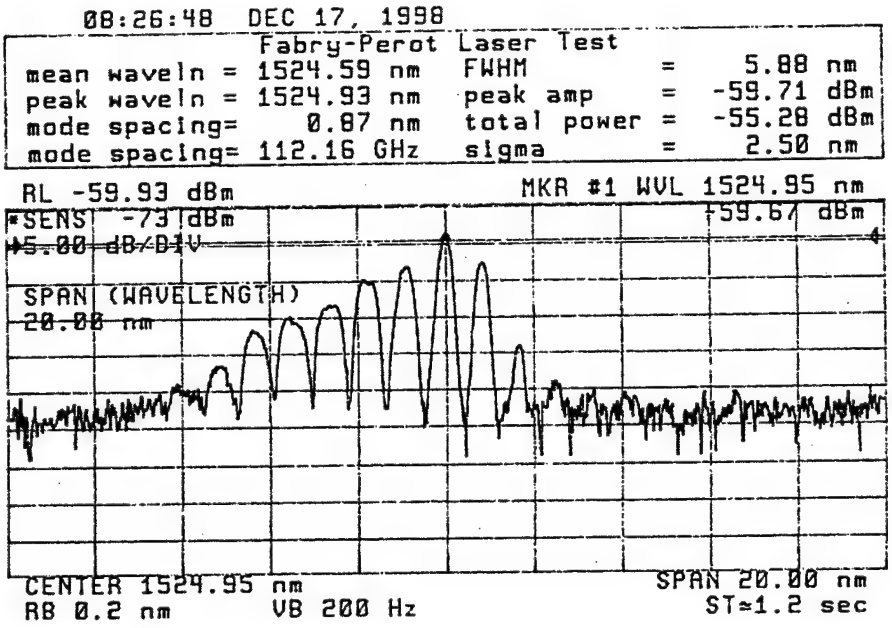

Figure 1.13: A representative spectrum of ridge-guide lasers fabricated from MR1080

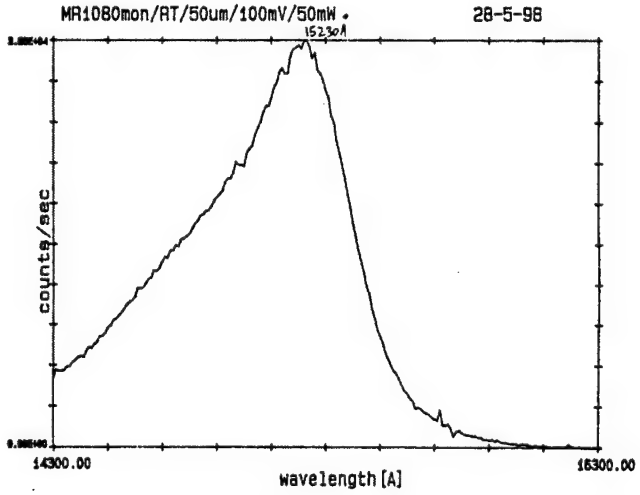

Figure 1.14: The room temperature photoluminescence characteristic of MR1080. The peak occurs at a wavelength of 1523 nm.

1.5 Conclusion

In this chapter work on the fabrication and testing of InGaAsP lasers has been presented. Material from the University of Sheffield, grown by MOVPE has been characterised using mesa stripe lasers.

Fabrication techniques for ridge-guide lasers have been developed, including controlled profile etching, electroplated contacting and bubble-etch wafer thinning. Ridge-guide lasers have been successfully fabricated using these techniques. The next steps in the work will be improvement of the P type contacting using e-beam evaporated Ti-Au and improved heat-sinking to enable CW operation.

Chapter 2: Quantum Confined Stark Effect in InGaAsP/InP Multiple Quantum Wells

2.1 Measurement of QCSE Induced Refractive Index Change in InGaAsP

The electrorefraction properties of InGaAsP/InP multiple qunatum wells must be explored to provide the design parameters for a QCSE tuned laser in this material system.

The absorption properties under bias were determined by measuring the photocurrent spectra with a white light source and a monochromator. A large area PIN diode was fabricated from the wafer MR1074 to allow biased measurements to be made. The epitaxial structure of the wafer used is shown in Figure 2.1. It consists of 60 InGaAs quantum wells with quaternary barriers.

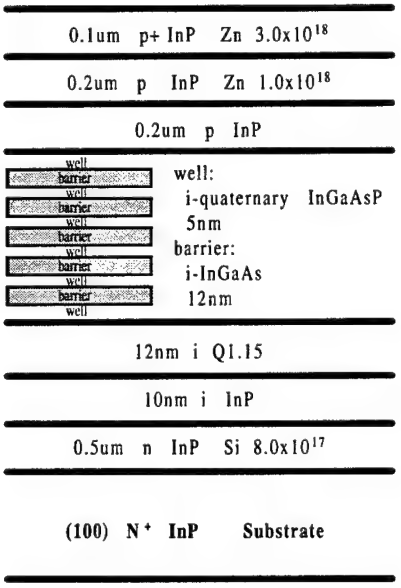

Figure 2.1: The Epitaxial structure of wafer MR1074

The differential absorption spectra were calculated directly from the absorption measurements. Given the measured change in absorption over a sufficiently large spectral range it is then possible to evaluate the change in refractive index that results from the measured change in absorption by using the well known Kramers –Kronig relationship between the change in absorption $\Delta\alpha$ and the change in refractive index Δn:

$$\Delta n(\lambda, E) = \frac{\lambda^2}{2\pi^2} P \int_0^\infty \frac{\Delta\alpha(\lambda', E)}{\lambda^2 - \lambda'^2} d\lambda'$$

where P is the Cauchy principal value of the integral, λ is the wavelength and E is the applied field.

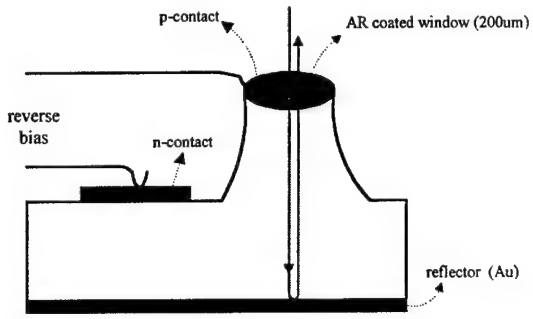

Figure 2.2: A Schematic of the PIN structure used to measure the photocurrent spectra of the MQW wafer MR1074. The device diameter is 200 μm for ease of optical access in the measurement arrangement.

The result of the absorption measurement is shown in Figure 2.3. Since there are a large number of quantum wells in this structure the applied field per well is relatively small and hence there is only a small shift in the position of the exciton absorption peak. The change in absorption calculated from the complete absorption measurement is shown in Figure 2.4 and the result of transforming that data into spectra of refractive index change versus wavelength using the Kramers-Kronig relation is shown in Figure 2.5. It is assumed that the change in absorption is zero outside the measured spectral bandwidth.

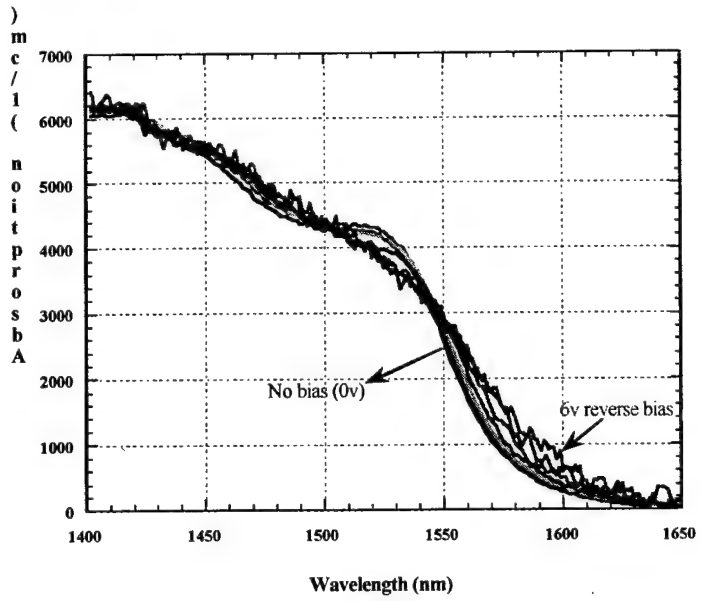

Figure 2.3: The absorption spectra for MR1074 as measured by the photocurrent method for applied bias from 0 V to –6V

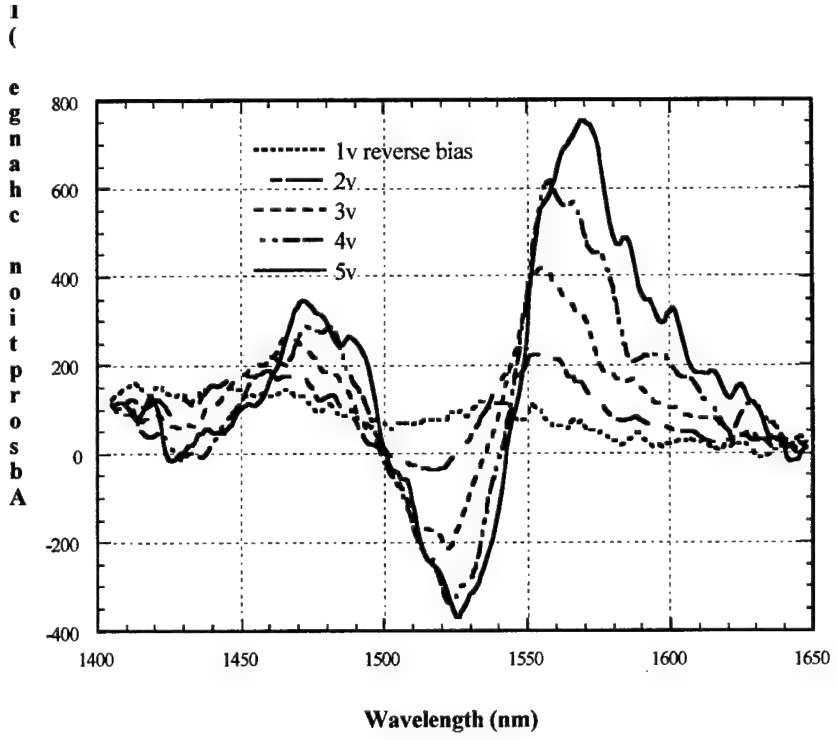

Figure 2.4: The change in absorption under applied bias for MR1074

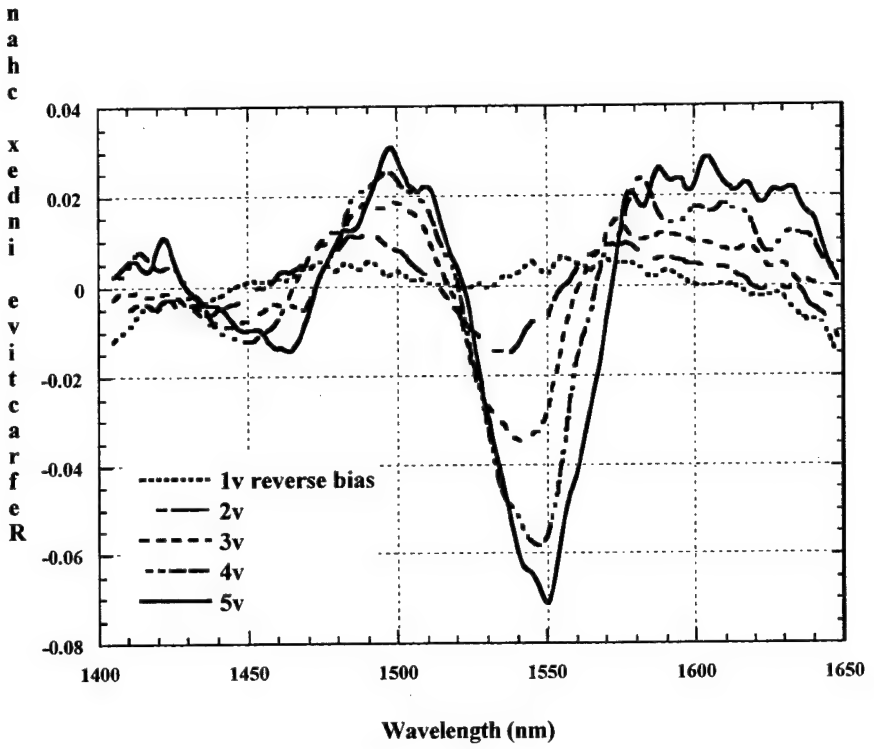

Figure 2.5: The refractive index change for MR1074 calculated from the absorption change via the Kramers Kronig transformation. It can be seen that over the wavelength region 1580nm to 1630nm the absorption loss is low and an index change of up to 0.5 % can be obtained.

2.2 Tuning Section Design for InGaAsP/InP Tunable Lasers

In a two section Fabry-Perot laser the relationship between the section lengths L_A, L_B, the wavelength λ, and the effective refractive index of each waveguide section n_{eA}, n_{eB} is:

$$2(n_{ea}L_a + n_{eb}L_B) = m\lambda \qquad (2.1)$$

where m is an integer. If the refractive index of the tuning section, B, changes, but not sufficiently to cause a mode hop, then continuous tuning can be obtained. The degree of static tuning obtained is given by:

$$\Delta\lambda = \frac{\Gamma\Delta n L_B}{n_{eA}L_A + n_{eB}L_B}\lambda \qquad (2.2)$$

where Γ is the optical confinement factor. The maximum continuous tuning range is given by the mode spacing of the resonator:

$$\Delta\lambda_{\max} = \frac{\lambda^2}{2(n_{eA}L_A + n_{eB}L_B)} \qquad (2.3)$$

A two section QCSE tuned laser operates with one section under forward bias as the gain section.

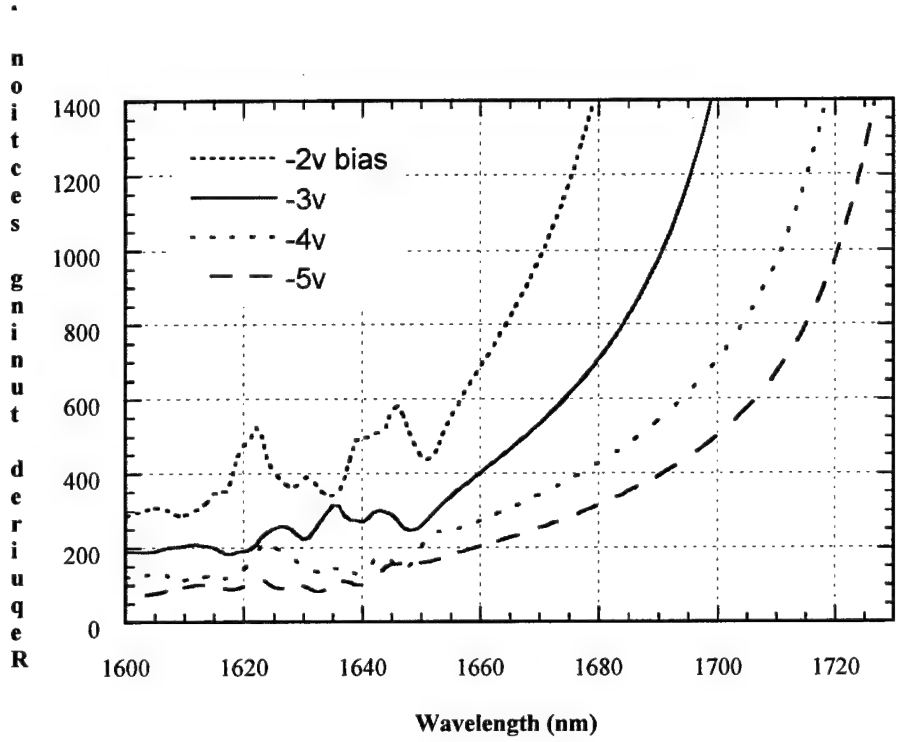

Figure 2.6: A calculation for the required length of a tuning section to ensure a π phase change with Γ = 0.2.

The other section is reverse biased and can be used for static tuning or optical FM transmission. The maximum tuning range is reached when the tuning section applies an additional phase shift of π. The tuning section length required for π phase shift is

$$L = \frac{\lambda_0}{2\Gamma\Delta n} \qquad (2.4)$$

where λ_0 is the oscillation wavelength, Δn is the refractive index change, and Γ is the optical confinement factor. In the case of the refractive index change determined for wafer MR1074 the

expected length of tuning section under different bias conditions to achieve a π phase shift is shown in Figure 2.6. In that figure the wavelength range chosen is offset from the e1-hh1 exciton peak, as would be necessary to reduce the insertion loss of the QCSE tuning section and avoid unintentional intensity modulation of the source with tuning.

The insertion loss for an absorption coefficient of α is

$$Loss = 10\Gamma\alpha L \log_{10} e \text{ (dB)}. \qquad (2.5)$$

In order to have low insertion loss and small absorption variation, the operating wavelength in the tuning section should be detuned significantly beyond the zero bias exciton absorption peak. In the case of MR1074 this means beyond ~1600 nm.

A long tuning section (> 1mm) will not be acceptable because of internal loss mechanisms and because high speed modulation will not be possible due to the large tuning section depletion capacitance.

2.3 Static Tuning Performance

For a specific tuning section length in a two section laser, the maximum frequency deviation that can be achieved is determined from the following expression:

$$\Delta v = \frac{c}{\lambda_0^{\,2}}\Delta\lambda = \Gamma\frac{c}{\lambda_0}\frac{\Delta n}{n}\frac{L_{tuning}}{L_{total\_cavity}} \qquad (2.6)$$

which is dependent both on the applied bias and the wavelength.

Figure 2.7 shows the result of calculating the maximum frequency deviation for a fixed field variation given by 3 V reverse bias. The maximum frequency deviation decreases with wavelength with the slope increasing with the tuning section length.

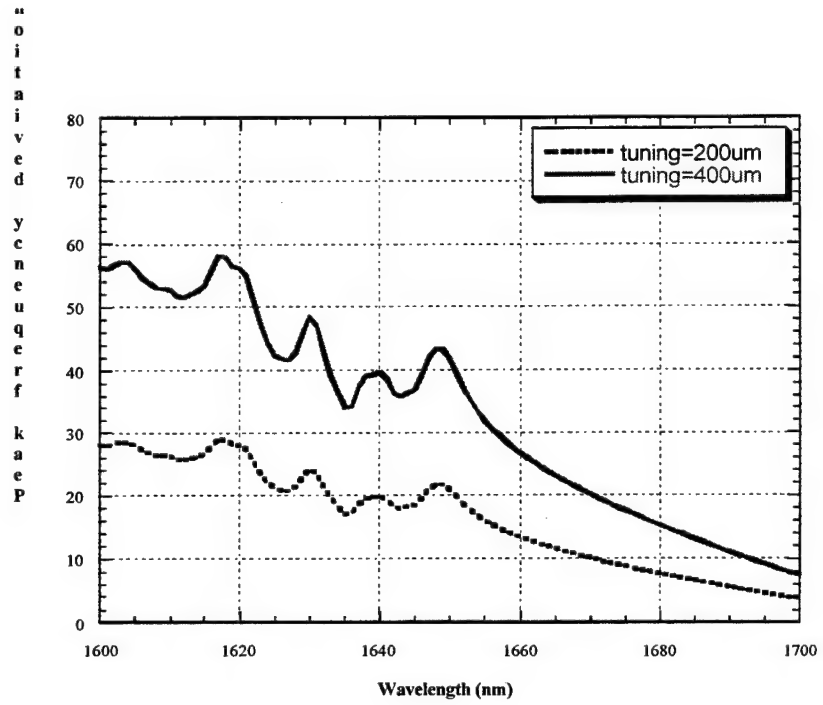

Figure 2.7: The maximum frequency deviation as a function of wavelength for an 800 μm long laser with tuning section lengths of 200 and 400 μm respectively. The bias level is assumed to be –3V with $\Gamma = 0.1$.

2.4 External Cavity Configuration.

A mask set has been designed to allow the fabrication of InGaAsP PIN normal incidence tuning elements, for external cavity QCSE tuned laser experiments. The diodes will be air-bridge contacted to minimise parasitic capacitance and allow operation of the modulator at microwave frequencies. Additionally, semi-insulating substrates (further reducing parasitics) will be accomodated by the mask set. A laser chip with one antireflection coated facet will act as the gain section while the normal incidence PIN diode will act as the tuning element. Figure 2.8 shows a cross sectional diagram of the tuning element.

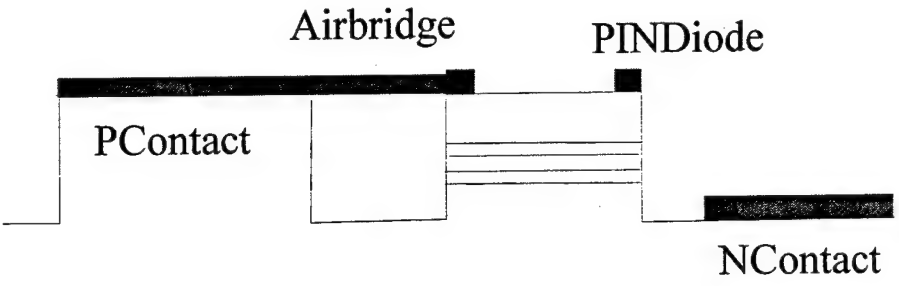

Figure 2.8: A Schematic of the modulator structure for microwave frequency applications. The airbridge reduces the parasitic capacitance of the contacts while using a small diameter mesa reduces the capacitance of the PIN structure.

The external cavity laser will be used as a vehicle to confirm the estimates of tuning range made above.

2.5 Conclusion

In this chapter we have described the fabrication of normal incidence test structures in the InGaAsP materials system to enable estimation of the tuning ranges obtainable and tuning element lengths required for the QCSE tuning mechanism. We have confirmed that element lengths of a few hundred microns will be sufficient for our application. We have also designed and fabricated a mask set for realising low parasitic capacitance normal incidence tuning elements. These will be used in an external cavity laser system to verify the tuning predictions made from the refractive index measurements.

Chapter 3 Dynamic Modelling of Multi-Section Lasers Using a Transmision Line Model

An important element in the development process for advanced optoelectronic devices is the availability of effective modelling tools. For design optimisation of single components or complete systems, computer based numerical models can help to predict or analyse behaviour before the design is committed to fabrication. This can yield time and financial benefits in a development cycle.

A dynamic model for a range of multi section lasers, based on a transmission line laser model has been developed [3.1]. Modelling results were obtained for a two section QCSE tuned Fabry-Perot Laser as described in Chapter 1, as well as for a fibre-grating laser with applications in mm-wave fibre radio systems. The model results show good agreement with the measured data. The model has also been used to predict the device characteristics of a gain-bandwidth restricted actively mode-locked fibre grating laser.

3.1 The Modelling Algorithm

The model used is based on the transmission line laser model derived from the well known transmission line modelling method for microwave circuits [3.2, 3.3]. The optical field in the laser cavity is represented by voltage pulses propagating on transmission lines. The simulation takes place entirely in the time-domain and so the frequency dependence of the gain must be represented by an electrical filter, which in this case is an RLC bandpass filter constructed from open and short circuit transmission line stubs. The spontaneous emission contribution to the optical field is modelled using a Gaussian random number generator.

The primary output of the model is a sampled version of the optical wave emerging from the laser facet, and a spectral representation of the output can be obtained by simply applying a Fast Fourier Transform (FFT) to the time segment of the output for which the spectrum is desired. The optical wave is in fact undersampled, which reduces the computational effort involved in

applying the model. Usually a bandwidth of a few Terahertz centered on the lasing wavelength is modelled, allowing one to obtain continuous spectra which cover all the modes and modulation sidebands within that bandwidth.

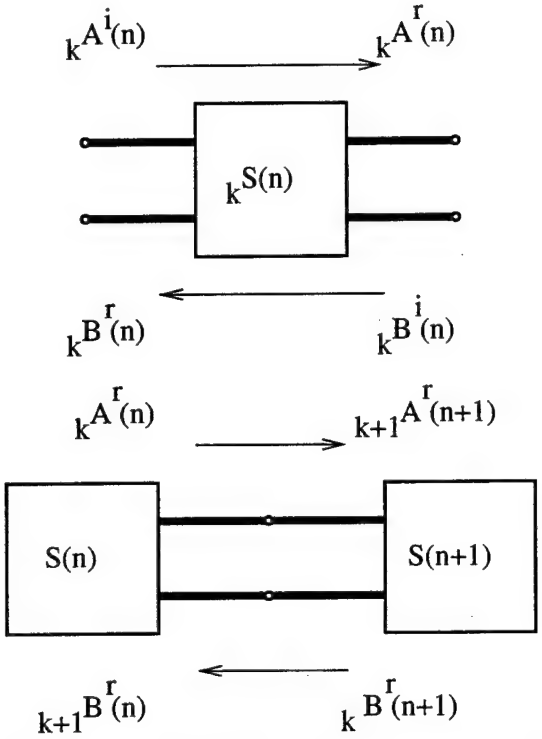

Figure 3.1: A schematic of how the optical wave propagates between scattering nodes.

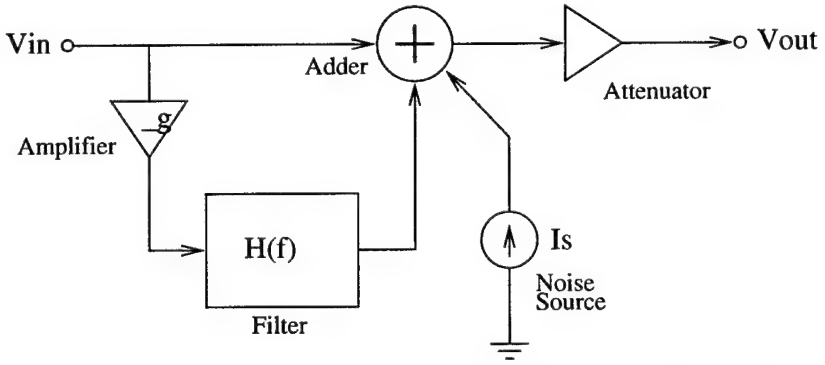

Figure 3.2: A schematic of the equivalent circuit representing the optical gain within a subsection.

In the longitudinal direction, the laser structure is divided into subsections of length ΔL, where each model subsection consists of a scattering node connected to the adjacent subsection by transmission lines, which are half a timestep long. Since the voltage pulses must arrive at the

scattering nodes synchronously, the model timestep ΔT is fixed in relation to the subsection length.

$$\Delta L = \frac{c}{\overline{n}_e} \Delta T \tag{3.1}$$

To model devices such as the QCSE tuned FM laser described in this report it is necessary to have a mechanism to model the changes in refractive index involved. The method applied is to introduce a complex phase shift to the forward and backward travelling waves at the appropriate subsections.

The actual simulation algorithm consists of two parts: scattering and connection. In the first part, the pulses which are incident on a subsection are scattered by applying a scattering matrix to produce the reflected pulses. The scattering matrix formulation embodies the necessary gain, loss etc. The second part of the algorithm models the propagation of the pulses in the structure, the reflected pulses becoming incident on the adjacent subsection in the next timestep. In each timestep the carrier density is calculated locally for each model subsection by forward integration of the carrier density rate equation and the photon density is calculated from the electric field in the subsection:

$$N_{t+\Delta T}(n) = N_t(n) + \Delta T \cdot \left(\frac{I_{inj}}{dwLq} - \frac{N(n)}{\tau_e} - \frac{S(n)c\Gamma G(N(n))(1-\varepsilon\Gamma S(n)}{\overline{n}_e} \right) \tag{3.2}$$

The scattering and connection process is illustrated schematically in Figure 3.1 while the gain model is shown in Figure 3.2.

The program has an object-oriented architecture and is implemented in C++ enabling efficient maintenance and extension of the code. Models for bulk and multiple quantum well gain sections, a phase-shifting tuning section, a passive waveguide and a Bragg grating are presently implemented and can be used to assemble complex laser structures for simulation.

3.2 Modelling Results

Modelling results have been obtained for three different types of laser device: a two-section QCSE tuned Fabry-Perot laser, a fibre grating laser designed for single mode operation and a gain bandwidth restricted actively modelocked laser (GRAM). Only the first two are relevant to the present work and results will therefore be restricted to these devices.

3.2.1 QCSE-Tuned Fabry Perot Laser

The two-section tunable laser is considered first. As we have described in Chapter 2 on the Quantum Confined Stark Effect (QCSE) in InGaAsP/InP multiple quantum well structures, the reverse bias voltage on the MQW structure allows tuning by QCSE. The center frequency of the model in this case is 349 THz but the results are applicable at other frequencies. Figures 3.3 to 3.6 show the transient response of the device to a step in current, the spectrum of the optical wave after the output has settled down and the spectrum of the device with a 6GHz modulating signal applied to the tuning section.

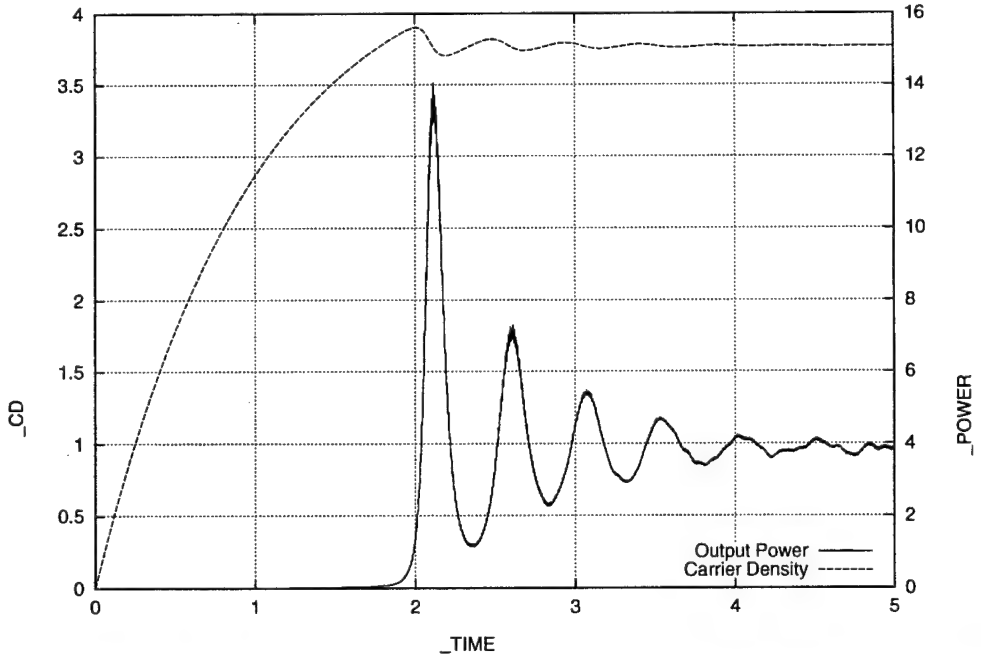

Figure 3.3: The transient response of the modelled two-section laser with 40mA drive current and no applied modulation (0 – 5 ns).

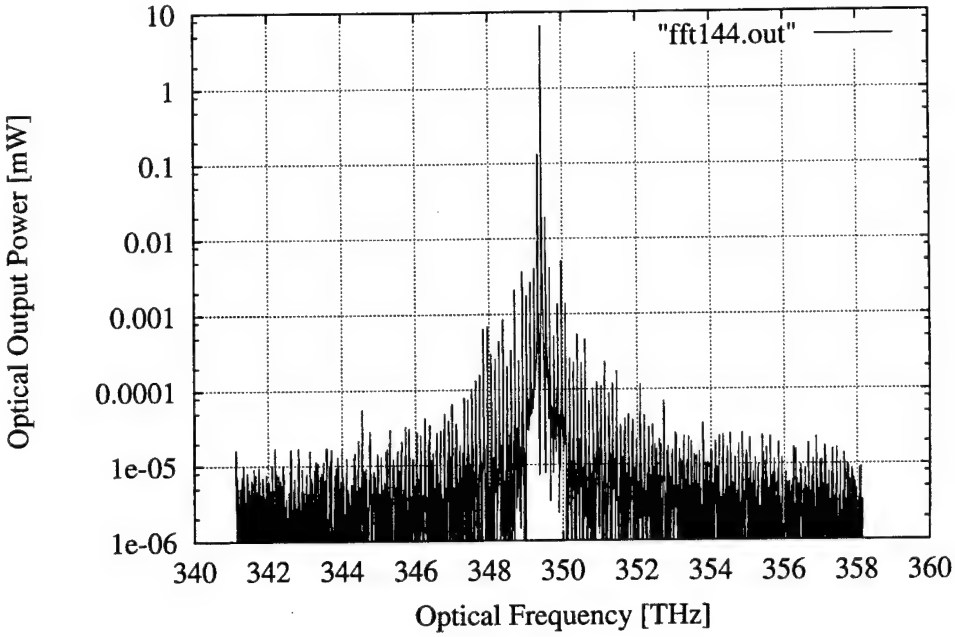

Figure 3.4: The spectrum of the two-section laser from 33.441ns to 33.678ns after applying current (Resolution =4.16 GHz).

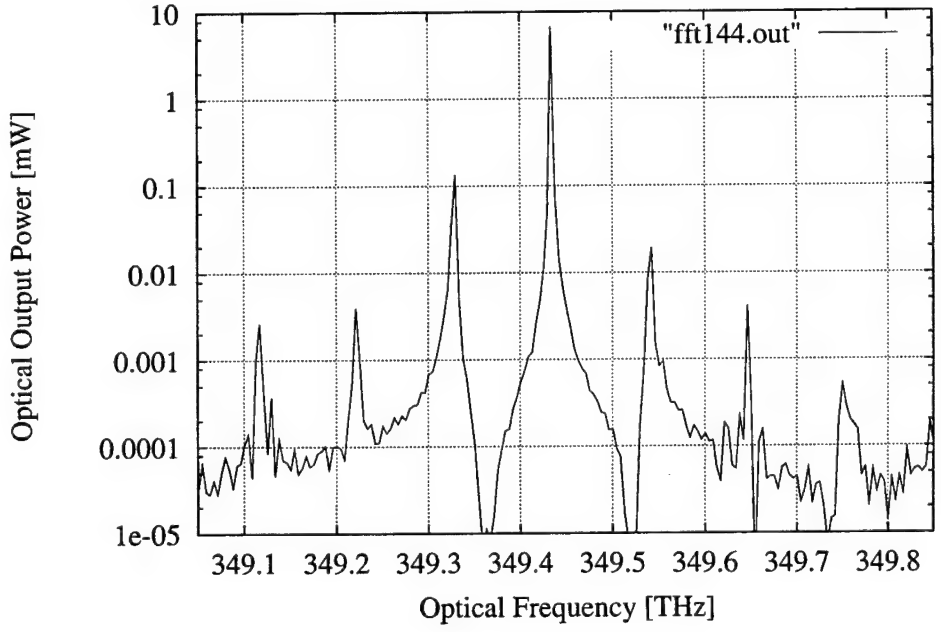

Figure 3.5: The same spectrum as in the previous figure showing the main mode and the first few side modes (Resolution = 4.16 GHz).

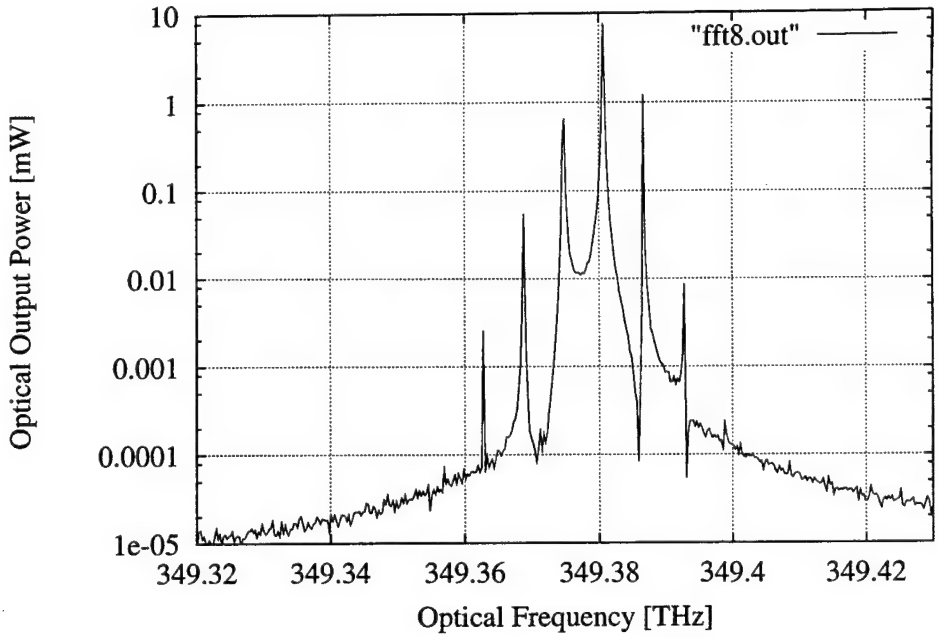

Figure 3.6: The main mode of the two section laser under 6 GHz modulation. (Resolution = 4.16 GHz)

3.2.2 Fibre Grating Laser

The second device to be considered is a fibre grating laser optimised for single mode operation. The setup comprises a standard laser with an anti-reflection coated facet which is coupled to a fibre Bragg grating [3.4]. The device modelled had a bulk gain section. The simulation results shown in Figures 3.7 to 3.9 include the transient response and the steady state spectrum as well as a spectrum for the device under modulation.

The potential of such devices is clearly shown in these figures. The narrow linewidth and excellent sidemode suppression (>45dB) are seen in Figure 3.8 while low chirp operation can be obtained under modulation as is shown in Figure 3.9. The FGL is a prime candidate as an optical FM source, due to its narrow linewidth, and should attract significant interest when combined with QCSE tuning elements.

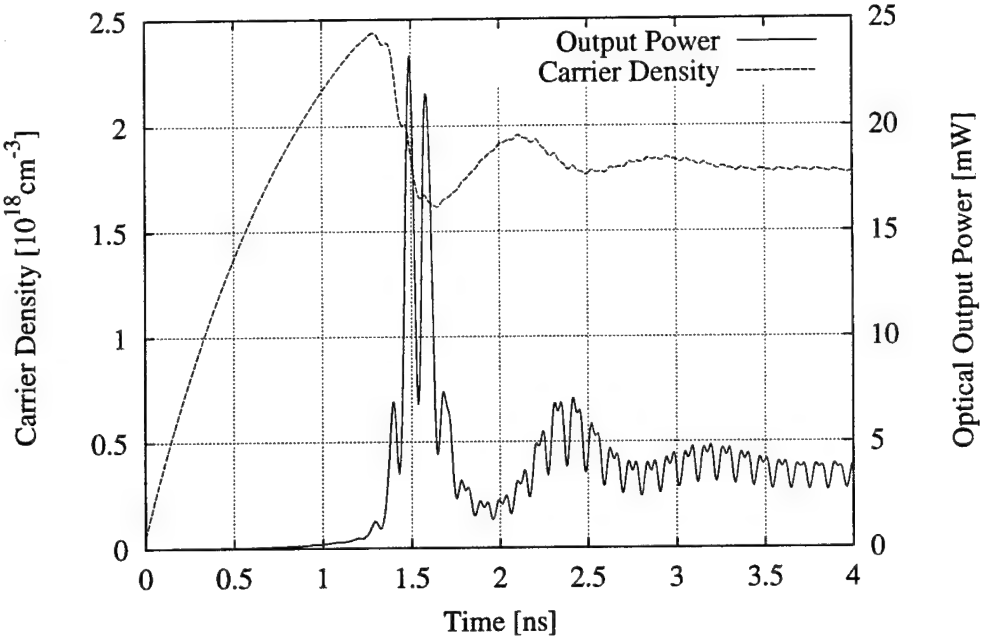

Figure 3.7: The transient response of a Fibre Grating Laser

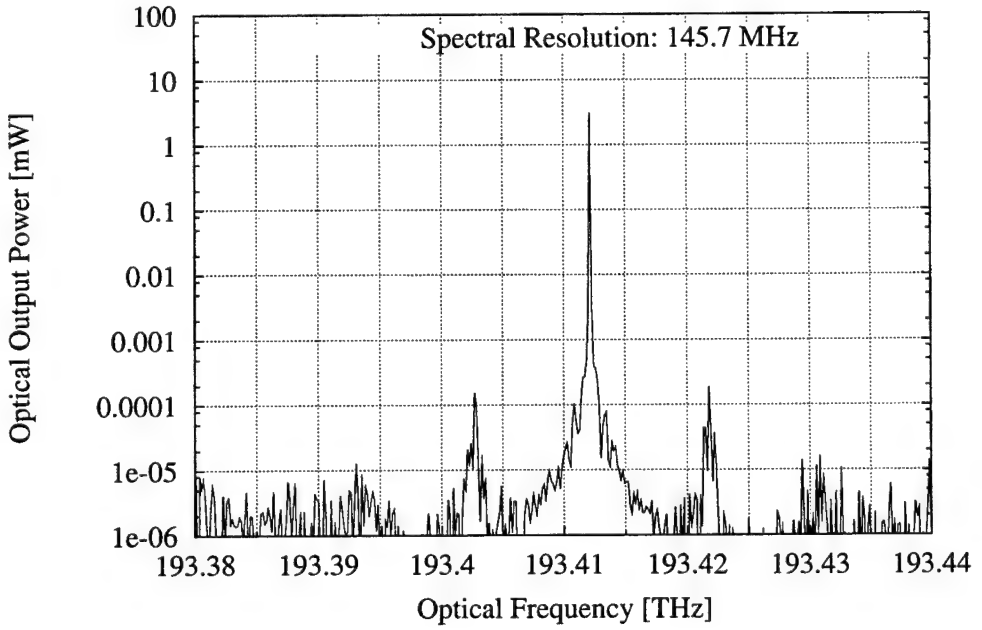

Figure 3.8: The spectrum of the Fibre Grating Laser under steady state output conditions.

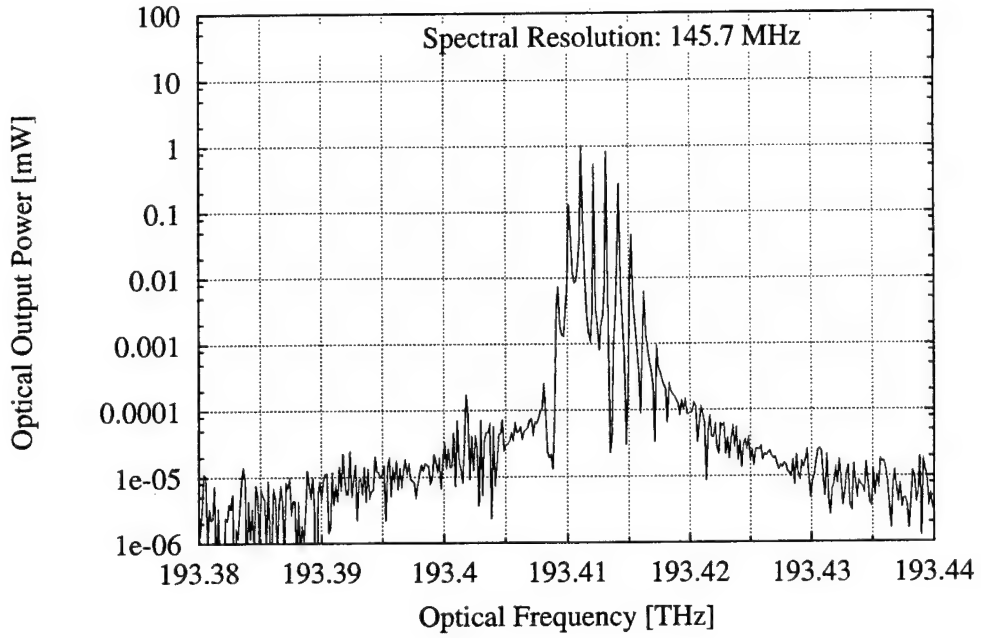

Figure 3.9: The spectrum of the central modes of the FGL under 1 GHz modulation

3.3 Conclusion.

The transmission line laser model has proven to be a useful tool in predicting the static and dynamic properties of a wide variety of laser structures. The model can easily be upgraded by the addition of new section types and the improvement of existing section types. It should prove to be a valuable addition to our design capabilities.

References

[3.1] O. Berger, " Dynamische Modellierung von Fasergitterlasern für die optoelektronische Mikrowellenerzeugung ", Diplomarbiet, Gerhard-Mercator-Universität Duisburg, FG Optoelektronik, June 1988.

[3.2] A. J. Lowery, "Dynamic modelling of distributed-feedback lasers using scattering matrices ", Electron. Lett., Vol. 25, pp. 1307-1308, 1989.

[3.3] A. J. Lowery, "Transmission-line modelling of semiconductor lasers: The transmission line laser model. ", Int. J. Numerical Modelling: Electronic Networks, Devices and Fields, 2:249-265, 1989.

[3.4] F. N. Timofeev, P. Bayvel, V. Mikhailov, O. A. Larova, R. Wyatt, R. Kashyap, M. Robertson and J. E. Midwinter, " 2.5 GBit/s directly modulated fibre grating laser for WDM networks" Electron. Lett. Vol. 33, pp. 1406-1407, 1997.

Chapter 4 Conclusions and Further Work

In this chapter we will review the achievements of our work during the contract and discuss briefly the next steps to be taken in exploiting the technologies we have developed to date.

4.1 Summary of Contract Achievements

In the first part of the work under this contract we developed the processing technologies for the GaAs/AlGaAs QCSE tuned laser to reduce the capacitance of the tuning section and so explore the wideband modulation capabilities of the QCSE tuning technique. We followed two approaches toward this end. The first was to use a planarised polyimide contacting technique on an N+ substrate. This successfully reduced the tuning element capacitance by at least an order of magnitude. However, contact adhesion was poor, making bonding difficult. The second was to use air-bridge contacting with a semi-insulating substrate. This reduced the tuning element capacitance to less than 2 pF, giving an upper –3 dB point in excess of 6 GHz in a 50 Ω source impedance system. Devices were easily bonded using conventional techniques. Using this approach we were able to demonstrate lasers with +/- 3 dB FM bandwidths of 30 kHz to over 6 GHz, a record for any field effect tuned semiconductor laser. The uniformity of the response was also demonstrated to be independent of laser output power and reproducible from laser to laser. This work resulted in a number of publications as detailed in Appendix A of the interim contract report. Further development of contacting techniques would allow the upper response limit to be extended to above 40 GHz, subject to round-trip-time limits, as described in earlier contract reports.

Turning to initial work in transferring the QCSE tuning technology to the InGaAsP material system, we have successfully fabricated normal incidence test structures to enable us to determine the electric field dependent QCSE-induced refractive index change. These devices were characterised using filtered white light and the index changes under bias determined by Kramers-Kronig transformation. We showed that it was easily possible to produce a refractive index change of 0.02 in a tuning element having acceptable (< 2 dB) loss. Thus FM with peak frequency deviation > 100 GHz should be possible with tuning voltages < 1 V.

We have also developed processing techniques for InGaAsP lasers. This work has included detailed evaluation of epitaxial material using wide (100 μm) mesa stripe lasers to determine J_{inf}, with the best results being obtained for strained-layer MBE material grown at the Laboratory for Physical Sciences. We did not proceed to the fabrication of ridge-guide lasers with this material since sufficient supplies were not available. We obtained J_{inf} of about 400 A/cm^2 using unstrained material grown at the University of Sheffield. Using this material we successfully developed processing technologies for a ridge-guide laser, although the fabricated lasers had rather high threshold currents (70 mA). Among the new processing technologies we developed to fabricate these lasers are plated P type contacts and bubble-etch substrate thinning. We are currently developing an MOVPE grown strained layer structure, with improved contacting and heat sinking to give low threshold operation. Thus, within the first year of our work on the InGaAsP system, we have demonstrated the viability of the tuning technique in this system by measurement of the QCSE induced refractive index variation and developed successful ridge-guide laser structures in the new system, which are suitable for the incorporation of QCSE tuning elements.

4.2 Future Work

4.3.1 QCSE Tuned Fibre Grating Lasers

In order to develop a narrow linewidth InGaAsP laser with high side-mode suppression, an extended cavity structure with strong longitudinal mode suppression is required. The modelling work of Chapter 3 has shown the attractiveness of the fibre grating laser (FGL) for this purpose. FGLs using bulk active region lasers have been investigated at UCL recently [4.2]. The fabrication of FGL devices will require minimal feedback from the facet coupled to the fibre grating. This will mean the use of an anti-reflection coating to minimise the intrinsic reflection of the waveguide facet and an angled ridge construction as shown in Figure 4.1 to further reduce unwanted feed back to the laser cavity. A mask set for the fabrication of the angled ridge-guide device should therefore be designed and fabrication of devices carried out.

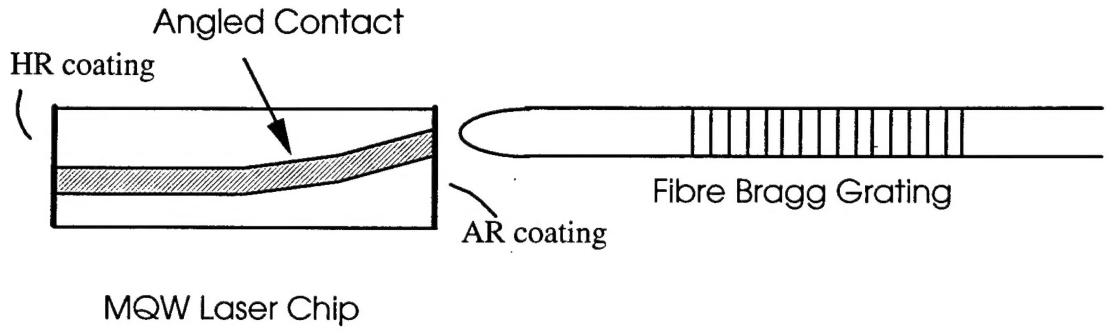

Figure 4.1: The configuration of the fibre grating laser (FGL)

The most significant development will be the incorporation of QCSE tuning to the laser. The anticipated route to this will be similar to that taken for the GaAs/AlGaAs monolithic tunable laser to give a two section device. To integrate monolithically a QCSE tuning section with a gain section will require post-growth band-gap engineering so as to minimise the loss in the tuning section[4.3-4.5]. The precise details of the mechanism to induce the desired Quantum Well disordering must be explored in a series of experiments conducted to isolate the optimal conditions. The final device would then be coupled to a fibre grating as shown in Figure 4.1.

4.3.2 Wavelength Agile Lasers for ATM WDM and Related Applications

The attractions of inter-packet tuning agility in wavelength division multiplexed networks are well recognised [4.6]. In our work on QCSE tuned lasers we have achieved the fastest field effect tuned lasers yet reported [4.1], with tuning speeds adequate for inter-packet channel hopping even in 10 Gb/s line rate Asynchronous Terminal Multiplex (ATM). It is natural therefore to apply the tuning technique to lasers with a wide tuning mechanism, through the use of QCSE tuned Bragg structures, particularly since the QCSE mechanism is free of the device to device irreproducibility, delayed thermal response and laser power dependence of approaches reported so far. Design work on wavelength agile lasers should be carried out, followed by an initial feasibility demonstration in a Bragg ridge guide laser.

References

[4.1] X Huang, A. J. Seeds, J. S. Roberts and A. P Knights, " Monolithically integrated quantum confined Stark effect tuned laserwith uniform frequency modulation response", Photon Technol. Lett. Vol 10 pp 1697-1699, 1998.

[4.2] F. N. Timofeev, P. Bayvel, V. Mikhailov, O. A. Larova, R. Wyatt, R. Kashyap, M. Robertson and J. E. Midwinter, " 2.5 GBit/s directly modulated fibre grating laser for WDM networks" Electron. Lett. Vol. 33, pp. 1406-1407, 1997.

[4.3] J.H. Marsh, "Quantum well intermixing", Semicon. Sci. & Technol. Vol. 8 pp. 1136-1155, 1993.

[4.4] A. Hamoudi, E. V. Rao, P. Krausz, A. Ramdane, A. Ougazzaden, D. Robein and H. Thibierge, " Controlled disordering of compressively strained InGaAsP multiple quantum wells under SiO_2:P encapsulant and application to laser-modulator integration", J. Appl. Phys. Vol. 78, pp. 5638-5641 1995.

[4.5] T. Miyazawa, H. Iwamura and M. Naganuma, " Integrated external cavity, InGaAs/InP lasers using cap-annealing disordering", Photon. Technol. Lett. Vol. 3, pp. 421-423, 1991

[4.6] S Kuwano, Y Tada and N. Shibata, "100 ps frequency switching without bit loss for a 10 Gb/s ASK modulated signal", Photon. Technol. Lett., Vol. 5, pp. 354-356 1993.

REPORT DOCUMENTATION PAGE

Form Approved OMB No. 0704-0188

1. AGENCY USE ONLY (Leave blank)	2. REPORT DATE	3. REPORT TYPE AND DATES COVERED
	July 1999	Final Report

4. TITLE AND SUBTITLE

Advanced Semiconductor Lasers Using Confined Stark Effect Tuning

5. FUNDING NUMBERS

F6170897W0204

6. AUTHOR(S)

Dr. Alwyn Seeds

7. PERFORMING ORGANIZATION NAME(S) AND ADDRESS(ES)

University College, London
Gower Street
London WC1E 6BT
United Kingdom

8. PERFORMING ORGANIZATION REPORT NUMBER

N/A

9. SPONSORING/MONITORING AGENCY NAME(S) AND ADDRESS(ES)

EOARD
PSC 802 BOX 14
FPO 09499-0200

10. SPONSORING/MONITORING AGENCY REPORT NUMBER

SPC 97-4063

11. SUPPLEMENTARY NOTES

12a. DISTRIBUTION/AVAILABILITY STATEMENT

Approved for public release; distribution is unlimited.

12b. DISTRIBUTION CODE

A

13. ABSTRACT (Maximum 200 words)

This report results from a contract tasking University College, London as follows: For this 12-month effort, the contractor will investigate the design and fabrication of multiple quantum well |(MQW) tunable lasers, using reverse biased quantum confined Stark effect tuning sections for use in the 1,550 wavelength telecommunciations window and studying their performance characteristics. The goal of the effort is to provide a monolithically integrated optical source capable of tuning and uniform frequency modulation to microwave frequencies for use in wavelength division multiplex (WDM|) systems, as well as a low chirp or controlled chirp source for wideband, directly modulated intensity modulation systems. the effort will focus on the use of InP/InGaAsP MQW lasers with ridge guide structures and electrically isolated reverse biased sections for fast tuning and modulation. The effort shall provide for the specification and manufacture of the MQW material, laser device design and processing, and an evaluation of the pertinent performance characteristics of the completed devices. The experimental performance will be analyzed to refine the theoretical device modeling approaches as well as the materials and device fabrication technologies. Specific areas to be address will include: (1) an investigation fo the QCSE induced refractive index variation in the InP/InGaAsP materials system leading to the design of optimized tuning/modulation sections fo the laser. (2) The development of an inter-section electrical isolation technique having negligible optical loss. (3) An investigation of tunable laser structures for the 1,550 nanometer wavelength range leading to the selection of a design compatible with relatively simple fabrication techniques. (4) The fabrication and evaluation of a prototype QCSE tuned laser.

14. SUBJECT TERMS

EOARD, Communications, Fibre Optics, semiconductor lasers

15. NUMBER OF PAGES

38

16. PRICE CODE

N/A

17. SECURITY CLASSIFICATION OF REPORT	18. SECURITY CLASSIFICATION OF THIS PAGE	19. SECURITY CLASSIFICATION OF ABSTRACT	20. LIMITATION OF ABSTRACT
UNCLASSIFIED	UNCLASSIFIED	UNCLASSIFIED	UL